Chapter

Radiation Fluxes Waveguide-Resonance Phenomenon Discovered in Result of X-Ray Nanosize Beam Formation Study

Egorov Evgenii Vladimirovich and
Egorov Vladimir Konstantinovich

Abstract

The work discussed shortly the experimental results, which was the waveguide-resonance mechanism relevation forerunner of characteristic X-ray radiation flux propagation. Technology of the planar air extended slit clearance preparation is presented. The methodology of X-ray beam parameter study formed by these slit clearances, which allowed to find the critical parameter answering for the radiation flux propagation mechanism change from the multiple external total reflections to the waveguide-resonance one, is described. Main features of the X-ray flux waveguide-resonance propagation mechanism were revealed. The self-consistent model of the mechanism is displayed with details. It is shown that the waveguide-resonance effect has universal character, and it reflects the fundamental nature phenomenon. The peculiarities of X-ray device functioned in frame of the phenomenon manifestation planar X-ray waveguide resonator (PXWR) and the increasing methods of its practical efficiency are discussed. The phenomenon practical application is presented concisely.

Keywords: X-ray flux, external total reflection, X-ray standing wave, coherence length, X-ray nanophotonics, planar X-ray waveguide resonator, waveguide-resonance propagation phenomenon, spatial coherence, angular divergence, partial angular tunneling effect

1. Introduction

The problem of X-ray beam formation with a minimal size cross section and a small angular divergence is the central problem of all X-ray diagnostical methods. The first real step for the solution of this problem was connected with the names of P. Hirsch and J. Keller suggested to form X-ray microbeams by employing the glass capillary [1]. More recently, the planar thin film waveguides have been offered for X-ray microbeam formation [2]. Authors of the work showed that the waveguide with a material media core for X-ray beam transportation can form small size beams, but the beam intensity attenuation was very great. In the direction, development similar investigations were carried out in a number of experimental works

[3–5]. Authors of these investigations have managed to obtain X-ray beams with a width of 100 nm, a height of some millimeters, and the total intensity near 5×10^7 photon/s in condition of the resonant synchrotron radiation coupling. The significant progress in these research works was achieved by switching over a study from coupling mechanism of the emergent beam preparation to the ones based on the radiation transportation by the core layer from input of the waveguide to its outlet. In result of the flux mode structure analysis, the phenomenon of an X-ray standing wave arising was mentioned [4]. The properties of X-ray beams formed by polycapillary optics systems have been intensively studied, too [6–10]. The optics of systems is based on the phenomenon of X-ray beam multiple total external reflections on the inner surface of a quartz capillary. Mono and polycapillary optics are the beautiful facilities for the formation of microsize beams. At the same time, the polycapillary optics is characterized by significant losses of X-ray beam intensity in the transportation process. The problem of X-ray flux intensity losses was the subject of a specific investigation [11]. Authors of the work studied the effect of capillary damages in result of X-ray beam influence. They demonstrated the linear worsening of X-ray beam transmission ability for the glass capillary with an increase of radiation dose. This effect is not significant for the quartz guides of X-ray fluxes.

In parallel with the traditional approaches to micron and submicron X-ray beam formation mentioned above, it has been discovered the specific technique of a superfine beam preparation by using the so-called "slitless" collimator [12–14] formed by two quartz plane polished plates mated together. Its device lets to form X-ray emergent beam with the visible magnitude of a radiation intensity compared with the incident beam intensity value [12]. Unfortunately, the study of this phenomenon and attempts of its practical application have been undertaken in recent years only [15, 16]. In fact, the slitless X-ray collimator represents the planar waveguide with a minimum size of an air slit. Width of the slit is defined by roughness and waviness levels of the collimator reflector plane surfaces. At the same time, the air core between guide claddings is the ideal waveguide channel from standpoint of the radiation flux intensity preservation. Similar waveguides with fixed and tunable air gaps have begun to find the practical application in the works of Zwanenburg group [17, 18]. Their waveguides with Cr claddings and air core can produce the emergent beam with a width of d = 500 nm, a height of h = 0.1 mm, and a total intensity of $J = 2.4 \times 10^7$ photon/s [17]. Great omission of these works consisted in the ignoration of X-ray standing wave arising in air core of their radiation guides.

The original glance on the problem of X-ray flux transportation by a planar extended slit clearance was presented in the works of Kawai group [19]. As opposite to the standing wave conception, authors included the specific notion about X-ray traveling waves or Yoneda wing. This approach has some grounding in theory [20, 21]. But these works left behind bracket the interference interaction between falling and reflecting fluxes.

Very strange approach was suggested by Dabagov for the description of X-ray flux transportation by a hollow quartz capillary [22]. Instead of the conventional conception connected with the multiple total external reflection mechanisms, author advanced the idea of "X-ray quantum subsurface channeling." We believe that the approach is not pragmatic since the channeling phenomenon offers a photon motion in the periodic potential, but the surface of amorphous quartz cannot produce the correct periodic field.

A number of publications with model description attempts of X-ray flux propagation through a narrow extended slit are presented in the literature [23–26]. These models are built on the working hypothesis that X-ray radiation is the planar monochromatic electromagnetic wave. But it is universally known that the realistic X-ray sources produce the quasimonochromatic radiation fluxes with λ_0 average wavelength and $\Delta\lambda$ monochromatism degree.

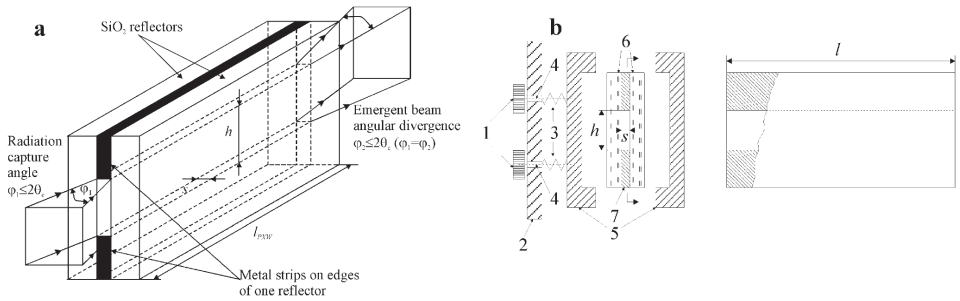

Figure 1.
Scheme of X-ray initial flux capture area and the emergent beam formation by the planar extended slit clearance formed by two quartz reflectors (a) and real construction of the device for the study of the spatial intensity distribution dependence in X-ray beams on the slit clearance width (b). 1: aligning handles; 2: installation plate; 3: spring pawls; 4: fine tuning screws; 5: radiation guide holder; 6: quartz reflectors with length 100 mm; h and s: height and width of slit clearance ($\varphi_1 = \varphi_2$).

Materials with information about $\Delta\lambda$ magnitudes featured for X-ray characteristic radiation produced by X-ray laboratory sources are presented in Handbook editions [27, 28]. But the main shortage at interpretation of X-ray flux transportation by different waveguide structures including slitless collimator devices was the statement that X-ray flux propagation takes place accordingly to the multiple total external reflection mechanisms as sole possible one. We were skeptical of this point of view and decided to produce the systematic investigation of the planar extended slit clearance width influence on its X-ray emergent beam parameters. For similar investigations, we selected construction presented in **Figure 1**. It is the air planar extended X-ray waveguide (PXW).

2. Technological features of PXW fabrication

The main components of the PXW structure are planar polished dielectric reflectors forming its radiation-transporting air slit clearance. In preparation of reflector working surfaces, it is necessary to fulfill a number of technological requirements guaranteeing the desired surface quality. The technical parameters that determine the surface quality are first of all the roughness and waviness and, moreover, a specific factor associated with local work hardening arising from nonuniform surface heating during polishing.

Modern polishing methods are capable of ensuring a surface roughness level of about 0.5 nm. Such a high degree of polishing can be controlled via direct testing with the help of atomic-force microscopy. The aforementioned roughness level is quite comparable with the range within which the potential on the condensed material surface varies from the value typical of its entire volume to that corresponding to vacuum [29, 30]. At the same time, the atomic-force microscopy technique makes it impossible to estimate the surface waviness and, moreover, the level and degree of surface distortions caused by the appearance of local work hardening. To a certain extent, the influence of these parameters on the surface quality can be estimated with the help of an optical method based on violated total internal reflection [31], which enables us to discard reflectors with appreciable contributions to the deterioration of the reflector surface quality.

In preparation of waveguide resonators, the most critical technological stage is thin film metallic strip deposition on the edges of one of the quartz reflectors constituting a pair used to create a waveguide-resonance channel. The deposited materials are titanium or chromium with a high degree of adhesion to the quartz surface. During the deposition process, the surface of the future waveguide-resonance

channel was coated with aluminum foil. Thin film metallic strips were primarily deposited in the vacuum chamber of a Leybord LG L-560 setup via the electron beam evaporation method. The film coating growth rate was 0.1 nm/s. During the deposition process, the chamber pressure was maintained at a level of 10^{-4} Pa. However, in spite of relatively high vacuum, the metallic-strip material contained a certain number of oxygen atoms (up to 10 at%). When the films were deposited, some reflectors were heated up to 80°C. As a result, the density of coating adhesion to the quartz glass surface increased appreciably. A simplified diagram of the mutual arrangement of assemblies in the chamber used to the deposit coatings in vacuum is depicted in **Figure 2**. The position of the reflector intended for coating deposition is symmetric with respect to the point source of metal atoms.

The basic requirement to the quality of the prepared strip coatings is thickness homogeneity along the entire length of the PXW reflector. Let us consider the geometry of the diagram, as shown in **Figure 2**. Then, under the assumption of angular homogeneity of the metal atom flux excited by the electron beam, it can be expected that the deposited strips will be characterized by a nonuniform coating thickness and its largest value will be at the reflector center. For coating deposition condition optimization, it is necessary to employ the thickness control methods. At the center (t_2) and edges (t_1) of the reflector (**Figure 3**), the deposited strip thicknesses were determined via the Rutherford backscattering (RBS) of He^+ ions with the help of "blank samples." Single-crystal silicon samples located on aluminum foil, which covered the surface during deposition, were used as these blank samples. Thus, each reflector with deposited metallic coatings can be characterized by at least two Ti/Si blank samples. Their experimental investigations were performed by means of the Sokol-3 ion beam analytical complex situated at the Institute of Microelectronics Technology and High Purity Materials, Russian Academy of Sciences [32]. The results of these measurements are depicted in **Figure 4**.

Using the spectra of the RBS of He^+ ions (E_0 = 1 MeV) (**Figure 4**), it is possible to perform accurate determination of the thicknesses of the strips deposited on reflectors in their central part (**Figure 4a**) and on the edges (**Figure 4b**). These thicknesses are determined by approximating peaks with almost flat tops, which

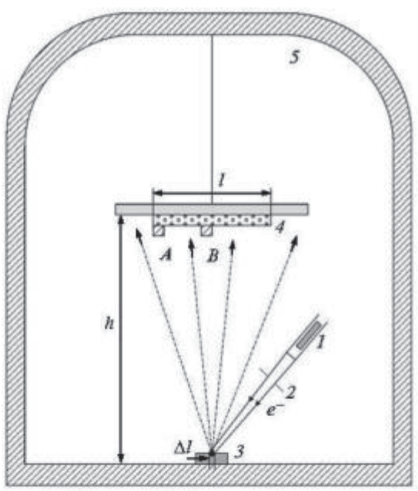

Figure 2.
Simplified diagram of the chamber used to deposit titanium strips on quartz reflectors: (1) electron gun, (2) focusing system, (3) titanium target, (4) quartz reflector, (5) vacuum volume, h = 200 *mm,* l = 100 *mm; and* A *and* B *are the positions of blank samples during deposition.*

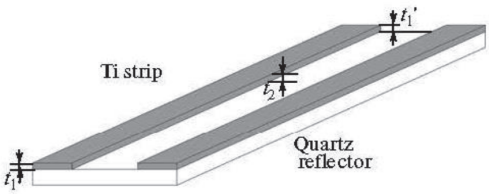

Figure 3.
Waveguide-resonator reflector with thin film strips on the edges: t_1 and are the coating thicknesses on its edges, and t_2 is the thickness in the central part.

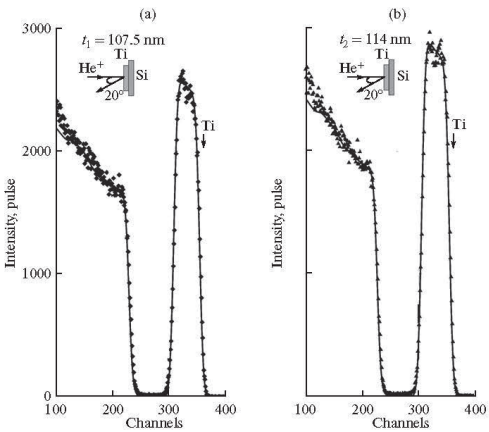

Figure 4.
Typical spectra of the RBS of He^+ ions (E_o = 1 MeV). Data were obtained for Ti/Si blank samples located at the positions A *and* B *(**Figure 2**) corresponding to the (a) edge and (b) center of the strip coatings of the quartz reflectors.*

correspond to He^+ ion scattering from the coating atoms. (The low energy steps observed in the RBS spectra of the tested targets correspond to He^+ ion scattering from substrate atoms.) The presented spectra were mathematically processed using RUMPP, the modified version of the famous RUMP approximation program [33]. Approximation of the aforementioned spectra indicates that the film strip thicknesses are t_2 = 114 ± 0.5 nm in the central part and t_1 = 107.5 ± 0.5 nm on the edges. Thus, the inhomogeneity in the thickness of the strips deposited onto the given reflector is 6%. This result completely coincides with the estimate based on geometric considerations. The above data correspond to the reflector whose coatings were deposited at a distance of h = 200 mm between the source of the evaporated atoms and its surface (**Figure 2**). The reflector length is l = 100 mm. Under the assumption that the deposition rate is proportional to the squared distance from the source, the expected difference turns out to be 6.1%. For the coating thickness difference decreasing, we increased the h-distance up to 1000 mm. In that case, the thickness difference accordingly to RBS data achieved to 1%. Experiments showed that the similar conditions are acceptable for X-ray waveguide assemblage.

Specific attention has been given to the direct determination of the effective slit width in different waveguides and in a slitless collimator because the data presented in early works about slitless devices [12–14] were not clear with respect to the width. The width was evaluated by very effective optical method connected with the attenuated total internal reflection effect [31]. In our investigation, we used the laser source with λ_0 = 680 nm. **Figure 5** presents the measurement geometry. The studied waveguide was situated in a specific cartridge equipped by black light absorber. The light beam introduced into the waveguide by using the quartz prism

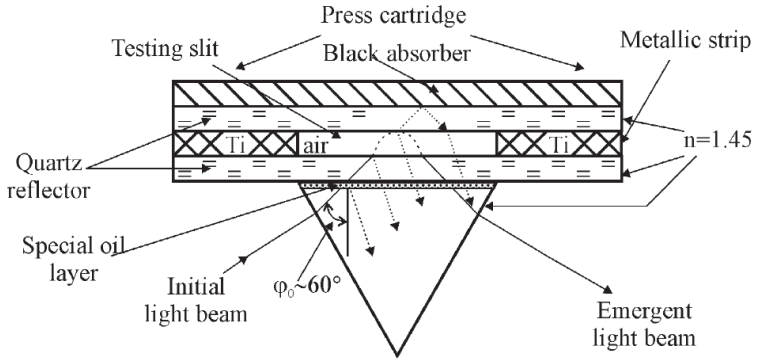

Figure 5.
Principle scheme for direct measurements of a waveguide slit width by methods of the attenuated internal total reflection (AITR). I and II are quartz reflectors of a waveguide. Scheme was published, in first, in Ref. [34].

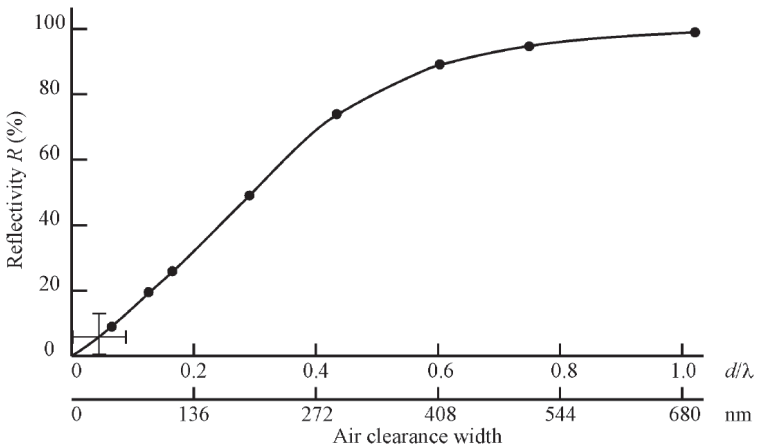

Figure 6.
Experimental data presented the relationship between the waveguide slit width and the reflectivity magnitude are obtained by AITR method. The point characterized the slitless collimator has a specific design.

fixed on the waveguide reflector by specific oil (n = 1.45). The prism could change its position on the reflector surface. Emergent light beam in the measurement process registered by standard photodiode equipped by circular aperture with a diameter of d = 0.5 mm. In the measurements process, the light beam in transit through the prism incidented on the waveguide, underwent the attenuated total internal reflection on the waveguide slit clearance and a lux meter recorded the reflection intensity. The normalization measurement was executed by using the waveguide with a width slit of s = 0.12 mm. Specific details of investigations are described elsewhere [34]. The measured data for several waveguides with different slit widths are presented in **Figure 6**.

Standard least square method was used for the experimental data fitting allowed to get a relationship between the light beam reflectivity factor and the width of waveguide slit clearance. In process of the slitless collimator study, we registered the gap width variation in interval 0–60 nm at the prism translation along the slitless unit. In result, we concluded that the slitless collimator is characterized by effective width of the gap $s = 30 \pm 30$ nm.

3. Experimental setup for the radiation intensity distribution study

The main device to study the X-ray intensity distribution was the HZG-4 diffractometer manufactured by Carl Zeiss Jena Firm. We produced some modification of the device by its detector circle radius increasing up to 500 mm. In the modification result, the measurement space resolution improved in three times. The measurement spectroscopic circuit was completed by NIM standard units produced by Ortec firm. The shaping time of amplifier unit was selected as 0.5 μs. Such selection allowed to get the pulse registration count rate up to 100 kHz. The design of our registration setup is presented in **Figure 7**. X-ray diffractometer used as the setup background is characterized by scanning regimes in nonstop function and start-stop moving with a minimum step of $\delta(2\theta) = 0.001°$. X-ray detector was equipped by slit-cut arrester with a width of $s = 0.1$ mm and a height of $h = 10$ mm and Soller slit system limiting the registered flux vertical divergence by value near 2°. X-ray flux take-off angle was selected near 6°. Main volume of experimental investigations was executed by X-ray tube BSW-24 (Cu) in regime $U = 20$ keV and $I = 10$ mA. Similar tube with Fe anode was exploited in some selective measurements. The X-ray space intensity distribution data collection was produced with the use of Cu filter attenuator characterized by the CuKα radiation decreasing factor $K = 200$. For the energy spectrum characterization, our facility setup was equipped by a pulse multichannel analyzer ACCUSPEC Canberra Packard in the form of PC computer board. In measurements of PXW parameters, we used the characteristic part of initial X-ray spectra only.

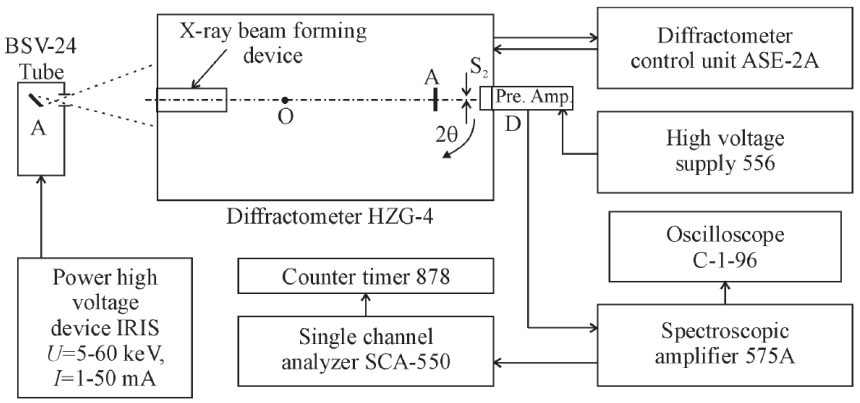

Figure 7.
Instrumental facility for the spatial distribution study of a quasimonochromatic radiation intensity in X-ray beams formed by quartz planar waveguides.

4. Angular radiation intensity distribution in X-ray beams

In the course of our measurements, the waveguide position in experimental setup in experimental process was not changed. In the experimental process, the distance between the waveguide inlet and the X-ray tube focal position was 75 mm, and the distance between the waveguide outlet and the X-ray detector slit was 460 mm. X-ray flux capture angle calculated on the basis of geometric approach was equal to 0.08° owing to the size of tube focus projection evaluated as 0.1 mm. In experiments, the diffractometer angular step $\Delta(2\theta)$ was 0.02°. At the same time,

the detector slit angular acceptance was 0.01°. The single channel analyzer during experiments transmitted only pulses connected with the Cu characteristic radiation. Scheme of experimental measurement is presented in top position of **Figure 8**. Experimental results are shown in bottom of **Figure 8**.

The slit clearance size interval $0 \leq s \leq 2$ μm was characterized by the absence of the intensity distribution profile transformations for waveguide emergent X-ray beams. Profiles of these distributions were beautifully described by the Gaussian function. It showed some differences in FWHM values and total intensity magnitudes. The intensity magnitude scattering is likely due to our polishing technology wretchedness, but its increasing at $s > 200$ nm is higher as the experimental error. The distribution FWHM was not exceeded the radiation capture angle. At the same time, when the slit clearance width had exceeded 3 μm, the space intensity distribution found new form, which could be interpreted as a set of lines. Experimental data of the waveguide emergent beam total integral intensity dependence on the slit clearance width are presented in **Figure 8**. These dependence can be described by three typical size interval: $s \leq 200$ nm (a), $200 \leq s \leq 3000$ nm (b), and $s \geq 3$ μm (c) with different characters of the dependence.

Registered experimental data and common sense allowed to assume that the X-ray waveguide emergent beam consists of some independent deposits. One can suppose by using the geometrical optics concept that one of them is connected with the X-ray beam direct propagation through the waveguide slit clearance without

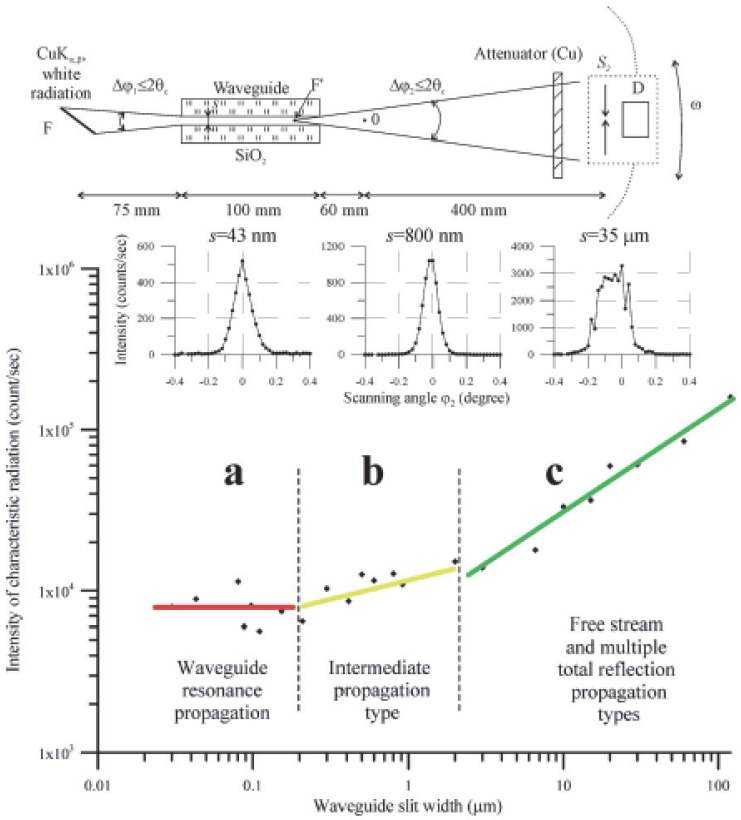

Figure 8.
Experimental scheme for the spatial distribution study of X-ray beam intensity formed by PXWs (1) patterns of $CuK_{\alpha\beta}$ intensity spatial distribution in beams formed by PXWs with slit sizes 43 nm, 800 nm, and 35 μm (2), and the experimental dependence of $CuK_{\alpha\beta}$ total intensity in beams formed by PXWs on its slit width (3).

waveguide reflector surface interaction. It is clear that at any width of the slit clearance, the direct beam will form its own partial peak and will show the linear dependence of its integral intensity variation on the slit clearance width. Its intensity will be equal to zero for the case of the slit clearance zero magnitude. Experimental data showed that the direct beam propagation mechanism was not able to describe the integral beam intensity variation dependence on the slit clearance width, especially, for the nanosize slit interval (a). In this region, the emergent beam total intensity maintains constant magnitude, which is more higher than zero. Calculations showed that the direct beam deposit into the experimental data magnitude for this region is less that 1%. Second region (b) is characterized by the monotonous integral intensity increasing at growth of the slit clearance width. This effect can be connected with a deposit increasing the direct beam in the total X-ray beam intensity. Third region (c) defined as $s > 3$ μm demonstrates sharp intensity growth at the width increasing. This area is characterized by an addition deposit appearing connected with X-ray beam multiple total external reflections on waveguide reflector surfaces. The slit clearance width increasing in this region leads to linear growth of intensity deposits defined by mechanisms of X-ray beam direct and multiple external total reflection propagations. The total integral intensity growth of the waveguide emergent beam break off when the slit clearance width exceeds size of the radiation source focus projection.

The experimental data comparison featured for different regions of the slit clearance width and peculiarities discussion of different mechanisms of radiation fluxes propagation insist us on conclusion that the nanosize region (a) is characterized by the specific waveguide-resonance manner of X-ray flux propagation [35]. Devices functioned in frame of the resonance manner we called the planar X-ray waveguide resonators (PXWRs) [29]. PXWR forms the X-ray quasimonochromatic flux as the indivisible ensemble with parameters, which are not depended from the slit clearance width and the initial distribution in radiation flux captured by the device. The waveguide mechanism of the X-ray quasimonochromatic flux propagation featured for the narrow extended slit clearance demonstrates the X-ray radiation density increasing and decreasing the irreversible losses. Angular divergence of PXWR emergent beam is equal to its radiation capture angle, and they cannot exceed twice value of the total reflection critical angle featured for the reflector material.

The slit clearance width intermediate interval (region b) is connected with two independent deposits into integral intensity defined by direct and quasiresonance beam propagation mechanisms. The increase of slit clearance ensures small growth of the beam integral intensity, but its radiation density diminishes. Spatial intensity distribution featured for this region shows a single-component form owing to small influence of the multiple total external effects on the emergent beam integral intensity. This effect deposit into the intensity becomes decisive factor when the slit clearance width exceeds critical value $s = 3$ μm (c). In this case, emergent beam divergence arrives its maximum $\Delta\theta = 2\theta_c$ independently from the device input aperture magnitude. The intensity distribution demonstrates multicomponent structure.

With practical point of view, it is very interesting to compare the radiation density parameter featured for PXWR and waveguides corresponding to "b" and "c" regions with similar parameter featured for X-ray beams formed by a conventional slit-cut device. The beam integral intensity on the slit-cut former output is more higher than one formed by different PXWs. But in the radiation density parameter, the planar extended waveguide structures are more effective. Direct comparison of the slit width is presented in **Figure 9**. Enhanced radiation density peculiar to X-ray beams formed by PXW is connected with width difference of the

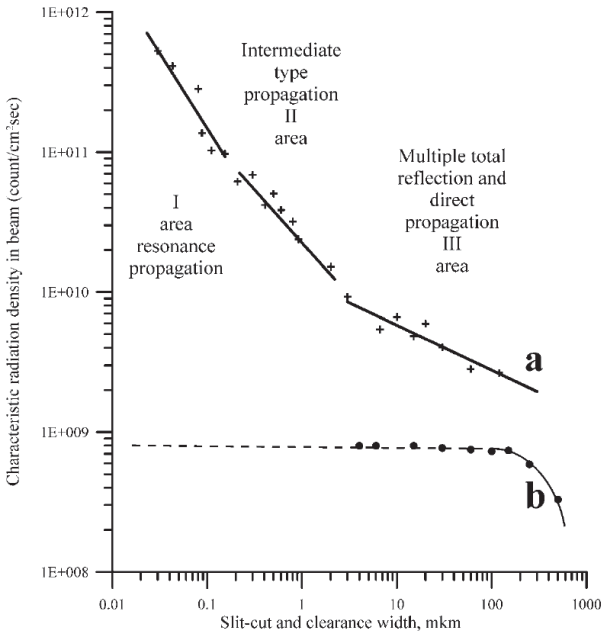

Figure 9.
Experimental dependences of CuKαβ flux radiation densities on slit width for X-ray beams formed by PXWs (a) and by the single slit-cut system (b).

waveguide slit clearance and the radiation source focus projection. Waveguides capture X-ray radiation fluxes in the angular aperture $\Delta\varphi \leq 2\theta_c$ from radiation source focus projection with width $P \sim 0.1$ mm into the slit clearance with more smaller width. In result, waveguide devices concentrate radiation. According to the data presented in **Figure 9**, PXWR is able to increase X-ray radiation density on three orders in its emergent beam in comparison with beams formed by slit-cut system. It is interesting that the maximum radiation density is expected for the slitless collimator. But the practical use of X-ray slitless system is troubled owing to the absence of the intensity stationary in its emergent beams.

5. Waveguide-resonance model for X-ray flux propagation

Figure 10a presents the idealizing scheme of X-ray flux total external reflection, which takes into account the degree of a radiation monochromatization $\Delta\lambda$ along

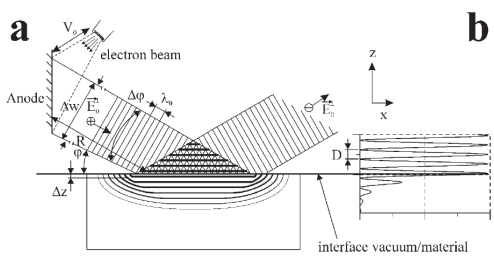

Figure 10.
Scheme of the interference field of X-ray standing wave arising from the external total reflection phenomenon in case of the quasimonochromatic flux interaction with material interface (a). Δw *is the source focus projection,* R *is the distance between X-ray source and target position,* φ *is the angular flux divergence,* Δz *is the penetration depth, and* D *is the standing wave period. Standing wave intensities in the air area and in the reflector volume (b).*

with the average wavelength λ_0. Owing to this principal limitation, the size of radiation standing wave area in the space over reflector will be bounded. $\Delta\lambda$ through the coherence length parameter characterizes the length of an electromagnetic radiation train or the photon longitudinal size. The interference phenomenon is possible if the path difference between the incident and the reflected fluxes does not exceed the magnitude of this parameter. But in any case, the longitudinal size of the interference area cannot exceed of the value. By this, it means that the coherence length of quasimonochromatic radiation is responsible for the longitudinal magnitude evaluation of X-ray standing wave area. In this framework of the phenomenological model, we accepted that the transverse size of the area is approximately equal to the longitudinal one. This premise is absolutely right so far as the real interference effect is connected with the spatial coherence of the quasimonochromatic flux radiation [36].

The next model postulate says that the description of the total X-ray reflection phenomenon must take into account the fundamental principle of a field continuity [37]. According to this principle, the interference field of X-ray standing wave cannot abruptly terminate on the material-vacuum (air) interface. The conventional model of X-ray beam total external reflection suggests that the radiation electromagnetic field amplitude undergoes exponential attenuation in the reflector material [38]. But the principle of electromagnetic field continually demands the exponential low multiplication on the interference term. Visualization of the modification is presented in **Figure 10b** and can be defined by the expression [39]:

$$\vec{E}_T(z,x,t) = \left[\frac{2\theta}{\theta + a + ib} e^{\frac{2\pi i z(a+ib)}{\lambda_0}}\right] e^{i\left(\omega_0 t - 2\pi p_x x\right)} \vec{E}_0 \tag{1}$$

where θ is the incident angle; λ_0 and ω_0 are the wavelength and the angular frequency of the radiation, respectively; p_x is the x-component of the photon momentum; and a and b are presented by the specific expressions [38]:

$$\left.\begin{aligned} a^2 &= \frac{1}{2}\left[\sqrt{\left(\theta^2 - 2\delta\right)^2 + 4\beta^2} - \left(\theta^2 - 2\delta\right)\right] \\ b^2 &= \frac{1}{2}\left[\sqrt{\left(\theta^2 - 2\delta\right)^2 + 4\beta^2} - \left(\theta^2 - 2\delta\right)\right] \end{aligned}\right\} \tag{2}$$

where δ and β factors are the formal parameters incoming into the conventional expression for the material refractive index [38]:

$$n = 1 - \delta - i\beta \tag{3}$$

The δ-factor is connected with the volume material polarization effect, and β-factor characterizes the attenuation degree of X-ray radiation flux in the material. But we would like to notice that the refractive index introduction in form presented by expression (3) is not correct, in principle. It suggests that the X-ray beam propagation velocity in material volume is higher than the velocity of the electromagnetic wave propagation in vacuum. Professor L.D. Landau at first pointed on this collision [40].

Figure 10a and **b** displays the principle model for an electromagnetic field distribution in the reflection area over and under the interface. The size of the interference area appeared over the interface is limited by the coherence radiation condition. But the interference area size under the interface is not limited. The entire volume of the reflector will be excited as a result of a flux total reflection on its local spot.

The external total reflection phenomenon is accompanied by an additional phase shift $\Delta\psi$ [41]. This parameter is the function of the flux incident angle φ. At the critical total reflection angle ($\varphi \cong \theta_c$), the additional phase shift strives to zero, but at the sliding incidence ($\varphi \cong 0$), $\Delta\psi$ value approximates to "π." The variation of the additional phase shift magnitude influences on the interference area size. Therefore, in framework of the waveguide-resonance model, the solution was accepted that the size of X-ray standing wave interference area is approximately conformed to half magnitude of the coherence length for the radiation flux undergoing the total reflection on the material interface [39].

If we place two planar dielectric polished reflectors on some distance, we can get the air planar extended slit clearance, which can be used for the realization of X-ray flux multiple external total reflection effects (**Figure 11a**). The consecutive multiple external total reflection phenomena are characterized by appearing the local interference area set. Since every elementary act of X-ray flux total reflection excites material volume of reflector, the next second reflection in the slit clearance on the reflector surface will lead to the material volume excitation. One can find specific X-ray flux incident angles, which will show the phasing of consecutive total reflection on every reflector (magic angles). Peculiarities of X-ray beam propagation through the air slit clearance are depended from the existence or absence of the phasing. The presence of phasing effect allows to transport the X-ray quasimonochromatic flux by PXW with small attenuation. The magic angle existence defines the discrete mode structure featured for the multiple total external reflection mechanisms. This picture is inherent for the X-ray polycapillary optics.

The mechanism of X-ray flux multiple total reflections is very efficient for the description of its propagation through planar wide slit clearances. But this mechanism is not able to characterize peculiarities of the radiation flux transportation by the super narrow planar extended slits. X-ray flux propagation through similar slits can be described on the basis of waveguide-resonance idea.

The conception of X-ray flux waveguide-resonance propagation is accompanied by appearing the X-ray standing wave uniform interference field in all narrow extended slit clearance spaces owing to the mutual overlap of local interference areas (**Figure 11b**). Overlay of these areas will be realized for any magnitudes of incident angles when it does not exceed the value of total reflection critical angle θ_c for the reflector material. The mode structure conception for PXWR is not existed. Moreover, we can confirm that the radiation coherence length magnitude is the critical parameter for the X-ray flux mechanism propagation change from the multiple external total reflections to the waveguide-resonance proceeding.

The narrow extended slit clearance radiation transport properties discussed above were investigated in the geometry when the projection of X-ray source focus was deposited in the symmetry plane of PXWR [39]. In this measurement geometry, the axis of X-ray incidence flux coincides with the axis of waveguide resonator.

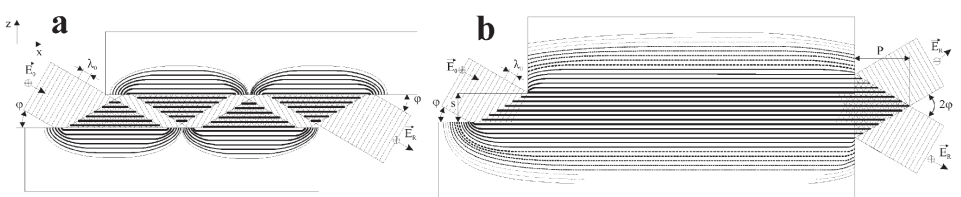

Figure 11.
Visualizating schemes of X-ray flux propagation through the planar extended slit clearance by the multiple total reflection mechanisms (a) and by the waveguide-resonance one (b). P *is the parameter of the interference field protrusion from PXWR slit.*

But in common case, the radiation flux can incident on the PXWR inlet at off-axis conditions. Measures in conditions of an initial X-ray flux off-axis incidence allow to differ the discrete mode structure from one with the continuous character, if the flux divergence is not great. The waveguide-resonance concept predicts that the off-axis incidence of X-ray flux will lead to the appearance of the emergent beam in the form of the double peak for a radiation spatial distribution (**Figure 11b**). The angular distance between the maximum of peaks must be equal to a double magnitude of the incidence angle. It is expected that the intensity of peaks must be approximately equivalent, and its divergences will be correlated with the radiation capture angle. Moreover, the integral intensity of the double-peak structure must be the monotonous function on the incidence angle for the angular interval $-\theta_c \le \theta \le \theta_c$. The reliable confirmation of all predictions following from the model of X-ray flux waveguide-resonance propagation was obtained in the course of our experimental investigations [36].

The integral intensity of PXWR emergent beam is insignificantly differed from the intensity of X-ray initial beam. Its magnitude can be described by the expression [39]:

$$W(x) = W_0 e^{-\alpha\mu x} \tag{4}$$

where W_0 is the initial beam intensity, μ is the linear absorption factor of reflector material for the radiation transported by PXWR, and α is the composite function defined by set factors of physical and geometrical nature. α magnitude is very small, and the attenuation of X-ray flux transported by PXWR is not significant. The experimental measurements showed that the attenuation factor for CuKα radiation transported by the quartz PXWR with a length of $l \sim 100$ mm can be near some per cents. The intensity losses for PXWR are smaller as the calculated values characterized for the multiple total reflection mechanisms. High radiation transportation efficiency of the planar X-ray waveguide-resonator is the result of the mode structure continuity for the flux propagating through its narrow extended slit clearance.

It is very important to notice that X-ray flux transportation by the waveguide-resonance mechanism is the result of the spatial coherence of quasimonochromatic radiation irradiated by X-ray tube. Owing to the fundamental physical reasons, a single X-ray photon in conditions of the total external reflection on the material interface cannot undergo interference with itself. The reflection process for X-ray and for other nature waves is accompanied by the Goos-Hanchen wave front displacement of the beam reflection position about the point of the beam incoming place, which is presented by the expression [42–44]:

$$\Delta x = \frac{\lambda_0}{\pi} \frac{1}{\sqrt{(\theta_c^2 - \theta^2) + 2i\beta}} \frac{1}{\sqrt{\theta_c^2 + 2i\beta}} \tag{5}$$

where θ_c is the magnitude of the total reflection critical angle. Minimum and maximum magnitudes of the displacement are arrived at $\theta = 0$ and $\theta = \theta_c$, correspondingly. The expressions for these values have forms:

$$\Delta x_{\min} = \frac{\lambda_0}{\pi\theta_c^2}; \quad \Delta x_{\max} = \frac{\lambda_0}{\pi\theta_c} \frac{1}{\sqrt{2\beta}} \tag{6}$$

Calculation of these factors shows that its magnitudes do not exceed the radiation coherence length and interference takes place.

6. Verification of the waveguide-resonance mechanism

The direct verification of the waveguide-resonance mechanism manifestation for the X-ray beam propagation can be found in the work of Japanese scientists [45]. The work was devoted to the transport property study of the angular structure as shown in **Figure 12a**. Japanese authors measured the MoKα flux intensity dependence on magnitude of the taper angle between two Si planar reflectors forming the radiation transportation structure. **Figure 12b** demonstrates the results of the measurements. The diffuse extremum *I* (near 0.1°) corresponds to reaching the critical total reflection angle for the molybdenum radiation on the silicon surface. The second extremum appearing near 0.007° cannot be explained without using the waveguide-resonance concept. The growth of X-ray radiation transport efficiency connected with this maximum reflects the transformation effect from the multiple total reflection propagations to the mechanism of the waveguide-resonance flux stream. The increase of an emergent beam intensity connects with a decrease in the flux attenuation featured for the waveguide-resonance propagation mechanism. The intensity of the second extremum is half of the first one, and the width of it is smaller than the first one on approximately one order. In result, the beam corresponding to the second radiation maximum will be characterized by the enhanced radiation density. The discussed results can be conceded as the independent confirmation of the waveguide-resonance mechanism objective reality for the quasimonochromatic X-ray flux propagation through the extended nanosize slit clearances.

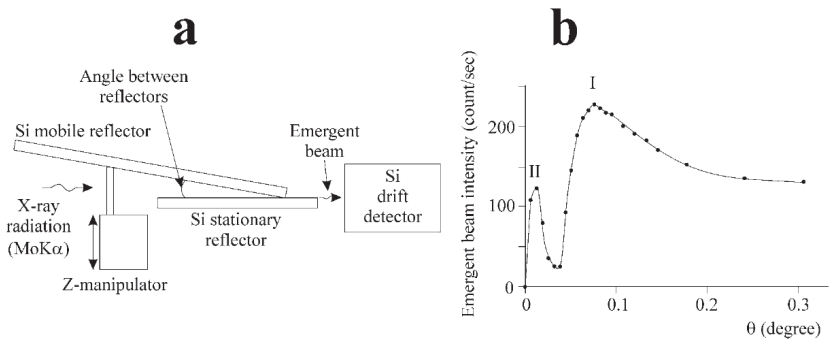

Figure 12.
Experimental scheme for the study of the radiation flux transporting peculiarities featured for the angular structure built on the basis of two Si reflectors under the variation of the taper angle between them (a), and the experimental diagram reflecting the emergent beam intensity dependence on the taper angle magnitude (b) [45].

7. Specific properties of PXWR

The waveguide-resonance mechanism is characterized by some specific properties of the quasimonochromatic radiation flux propagation through narrow extended slits, and the coherence length parameter is the limiting factor for the mechanism realization. The white radiation generated by X-ray tube is not characterized by parameter of the coherence length owing to the nature of this radiation arising [46]. But the experimental data presented in **Figure 13** show that the white radiation is transported by PXWR. At the same time, its related deposit at the total intensity of X-ray beam formed by PXWR is smaller than one in the beam formed by slit-cut system. So, one can expect that the spatial coherence degree for the white

radiation generated by X-ray tube is smaller than this parameter featured for X-ray quasimonochromatic lines. **Figure 13** shows that the white component intensity falls down approximately two times in all spectral ranges investigated in the experiments. Thus, a planar X-ray waveguide resonator cannot be considered as a restrictive filter for the hard white radiation. But PXWR application for X-ray beam formation decreases the white radiation deposit in the total beam intensity. This effect will be greatest for the smallest slit clearance width. The specific feature of PXWR is the impossibility to use it for β-filtration of X-ray tube initial radiation. The β-filtration procedure for X-ray diffractometry is well known [47]. This procedure is based on the use of the thin film absorber manufactured from the material, which is characterized by the energy absorption edge intervened between EK_α and EK_β of the tube characteristic radiation. Similar β-filter can be built on the basis of planar monocapillar prepared by using the dielectric reflectors containing a significant concentration of atoms characterized by a suitable value of the energy absorption edge. Our direct experiments showed that the similar approach is not right for PXWR. β-Radiation flux excites the uniform interference field of X-ray standing wave in all space of PXWR air slit clearance, and the intensity attenuation is not observed.

Specific properties of PXWR are not exhausted by the peculiarities discussed above. For example, the beam formed by the waveguide resonator has the nanosize width and the enhanced radiation density. The beam is not accompanied by diffraction satellites and can be modulated by an external influence. But the planar X-ray waveguide resonator is characterized by two serious lacks. The angular divergence of the beam formed by PXWR of the simplest design is usually near 0.1°, and its real integral intensity is smaller than the integral intensities of beams formed by the slit-cut systems and the polycapillary optic devices on 1–2 orders [39]. The angular divergence of PXWR emergent beam can be decreased without influence on its integral intensity by application of PXWR with specific design, which has name as the composite planar X-ray waveguide resonator (CPXWR) [48].

Figure 14 presents the results of comparative investigations of X-ray characteristic beam formation by PXWR with the simplest construction (a) and CPXWR (b). Left part of the figure presents the measurement schemes. Spatial distributions of X-ray intensities in beams formed by these devices are shown in the right part of the figure. Radiation capture angle is the same and is equal to $\Delta\varphi_1 = 0.11°$. Composite

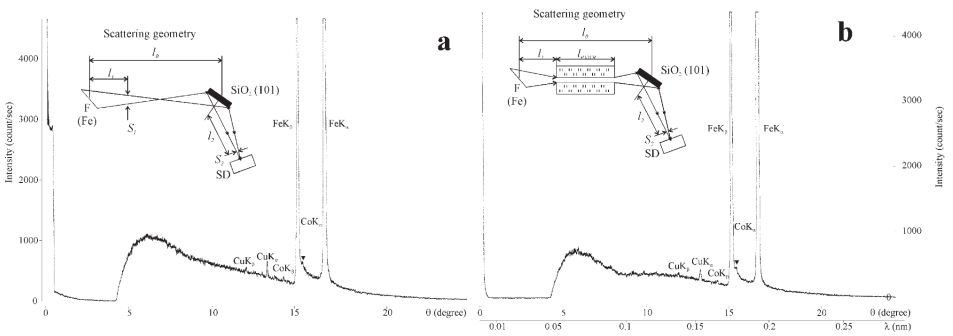

Figure 13.
Experimental diffraction patterns for SiO_2 (101) monocrystal specimen collected in conditions of a standard Bragg-Brentano geometry (a) and a waveguide-resonator application for the initial beam formation (b). The pattern normalization was carried out on the basis of equivalence of characteristic line intensities. Pattern (a) was registered at BSW-24 (Fe) X-ray tube regime U = 25 *keV,* I = 3 *mA and pattern (b)* U = 25 *keV,* I = 9 *mA. Geometrical sizes at the measurements were (a)* l_0 = 235 *mm,* l_1 = 50 *mm,* l_2 = 235 *mm,* $S_1 = S_2$ = 0.1 *mm and (b)* l_0 = 235 *mm,* l_1 = 50 *mm,* l_2 = 155 *mm,* l_3 = 85 *mm,* S_1 = 0.1 *mm,* s_{PXWR} = 0.1 *μm. The collection was carried out without a pulse discrimination.*

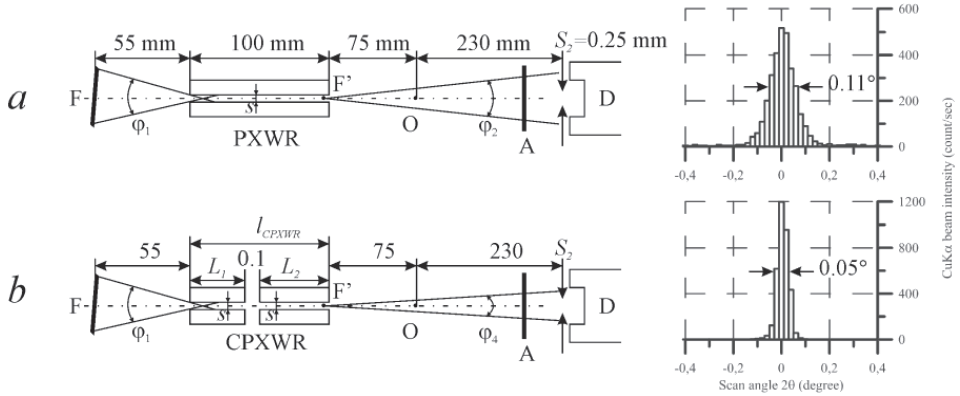

Figure 14.
Experimental schemes and flux intensity spatial distributions for CuKαβ beams formed by PXWR (a) and CPXWR (b) [48]. $S_{PXWR} = S_{CPXWR} = 88$ *nm,* $L_{PXWR} = L_{CPXWR} = 100$ *mm,* $l_1 = 75$ *mm,* $l_2 = 60$ *mm,* $l_3 = 400$ *mm,* $S_1 = 0.1$ *mm,* $L_1 = L_2 = 50$ *mm,* $\Delta L = 0.1$ *mm. Source regimes of BSW-24 (Cu) for both measurements* $U = 20$ *keV,* $I = 10$ *mA,* A – *filter attenuation factor* $K = 200$.

waveguide resonator differs from PXWR with the simplest construction by gap existence $\Delta L \sim 0.1$ mm between two PXWRs with the simplest construction built on the basis of short reflectors. The divergence of the waveguide emergent beams was studied by the method of the step-by-step detector scanning. The angular size of the detector slit S_1 was near 0.01°. The scanning step was $\Delta(2\theta) = 0.02°$.

Experimental intensity distributions for the beams formed by the conventional and the composite PXWRs demonstrate the Gauss form of distributions. FWHM of the peak distinguished for PXWR is $\Delta\varphi_2 = 0.11°$. At the same time, the magnitude of this parameter for CPXWR emergent beam is $\Delta\varphi_2 = 0.05°$ only. Total intensities of the peaks are approximately the same. Data presented show that the gap existence leads to the beam angular constriction without intensity losses. Such result is very alike on existence of the tunneling effect in the gap space. The increasing of ΔL distance up to 10 mm has led to an abrupt decrease of the peak total intensity and its FWHM.

Using the modified reflectors for the waveguide-resonator building allows to solve the second PXWR problem – low integral intensity of its emergent beam. Standard quartz glass plates modified by 30 mm polished tapers with an angle of $\psi = 0.5°$ were used for building the specific waveguide resonator (**Figure 15b**). For further radiation gathering power enhancement, the tapers were coated by HfO_2 thin film. Then, Ti strips with 90 nm thickness were deposited onto one plate edges, and the waveguide-resonance structure with a slit channel width of 90 nm and a height of 4 mm was assembled. In result, we received the skewed input concentrator with an angular aperture near 1°. Next, the comparative measurements of the conventional PXWR and the modified waveguide resonator were executed. The geometric parameters of the measuring schemes are given in **Figure 15**. Intensity spatial distributions for beams formed by the tested devices are shown in the same figure. In addition, the values of the total intensity (with and without the use of attenuator A) and the angular divergence of the beams are also quoted therein. The distributions were obtained at radiation source operation conditions [BSW-24 (Fe), $U = 20$ keV, $I = 10$ mA].

The data show that the envelope shape and FWHM of the intensity spatial distribution for a quasimonochromatic component of the beams formed by the conventional and the modified PXWR are nearly the same. On the other hand, the total intensity of the beam formed by the modified waveguide resonator is substantially higher than the beam intensity formed by the conventional PXWR. The data

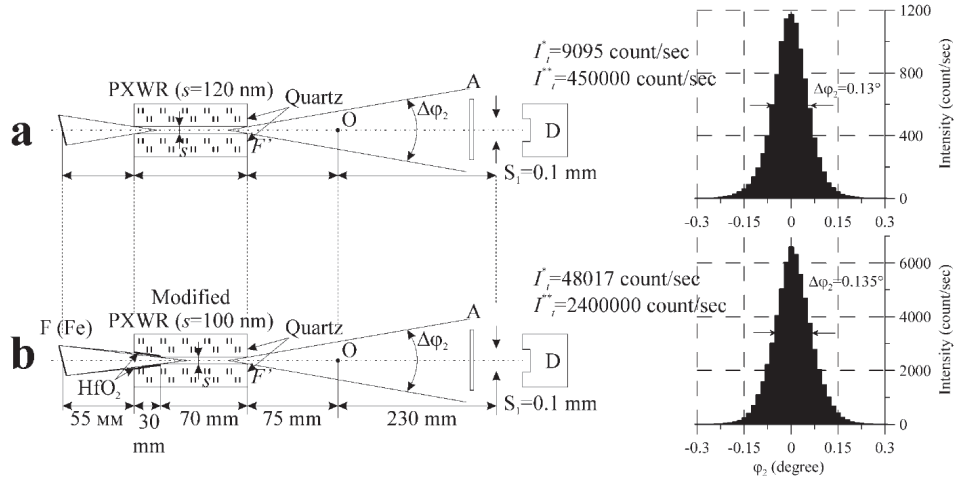

Figure 15.
Experimental schemes for the study of the intensity spatial distributions in X-ray beams formed by the waveguide resonator of a conventional construction (a) and PXWR with specific design (b) and real intensity distributions in its emergent beams. I^{*} *is the measurement magnitude, and* I^{**} *is the intensity corrected by taking into account the attenuator (*A*).*

show a fivefold increase in the radiation gathering power of the waveguide resonator due to the application of the input skewed radiation concentrator. Experimental value of the radiation gathering power enhancement obtained in our measurements was somewhat less than the rating. It is presumably explained by the nonoptimal length and form of the tapers. Nevertheless, the above result allows to state that the application of the input skewed concentrator is a powerful tool for the radiation gathering power enhancement of the waveguide-resonance structures, which provides the system modification without a significant loss in other parameters of the emergent beam.

In principle, there are other methods for the improvement of waveguide-resonator parameters. The most drastic method of PXWR parameter modification is the building of the multi-slit waveguide-resonance structures. According to our opinion, this way is very perspective, but it entails serious problems connected with the interference effect between the individual beams [49].

8. Practical application of the phenomenon

Experiments showed that the phenomenon of X-ray flux waveguide resonance increases the efficiency of X-ray fluorescence material analysis in conditions of exciting beam total reflection on studied surface (TXRF) [50]. This method modification by PXWR including the setup of TXRF spectrometer allowed to decrease the pollution detection limits in comparison with the convention of 1–2 orders. PXWR uses in experimental scheme of the particle induced X-ray emission (PIXE) allowed to elaborate the new experimental method for surface material element diagnostic [51]. Moreover, in some specific geometries, the method can provide element surface analysis being free from matrix effects.

The waveguide-resonance propagation of X-ray characteristic radiation fluxes can be achieved not only in frame of the external total reflection phenomenon but also at the use of the Bragg reflection. By using the Bragg-Laue waveguide-resonance cell (BLWRC), it is possible to build the pulsed X-ray laser on table, which will be useful for the study of kinetic processes [52]. Based on the use of

phenomenon consequences, it is possible to realize the reactions of cold nuclear fusion [53]. But the more important result of waveguide-resonance radiation propagation phenomenon discovery, we regard the possibility appearing to elaborate the function correct model for optical fibers and waveguides of light beams. Conventional model of its function is based on the light flux notion as the infinite plane wave and on the light flux transportation mechanism by planar symmetrical waveguide as the multiple internal total reflections in frame of the geometrical paradigm [54–63]. Similar approach is not right, in principle. It is well known that any radiation source generates quasimonochromatic beams with λ_0 mean wavelength and $\Delta\lambda$ monochromatization degree. So, any quasimonochromatic beam is characterized by the coherence length parameter. Up-to-date optical lasers generate the beams with several tens of meters of coherence length. Owing to the core size of planar symmetrical optical waveguides varies from some micrometers to some millimeters, we can conclude that all optical waveguides and fibers are functioned in frame of the waveguide-resonance phenomenon manifestation, and instead of mode structure, it is a need to discuss the properties of uniform interference field of optical radiation standing wave.

9. Conclusion

The paper presented some experimental results allowed to consider that the waveguide-resonance conception is right. We described the features of the waveguide-resonance mechanism discussed its principle model and fixed the critical parameter being responsible for mechanism change of the radiation flux propagation. References presented allowed to understand some practical application of the phenomenon and its consequences. The paper contains the short description of X-ray device functioned on the basis of mechanism – the planar X-ray waveguide resonator, the discussion of PXWR properties, and the ways of its construction perfection.

Acknowledgements

The authors would like to thank Prof. J. Kawai and Prof. R. Van Grieken for the great attention to the waveguide-resonance direction of X-ray optics and Dr. M.S. Afanas'ev for help.

DOI: http://dx.doi.org/10.5772/intechopen.93174

Author details

Egorov Evgenii Vladimirovich[1,2,3*] and Egorov Vladimir Konstantinovich[1]

1 Institute of Microelectronics Technology Russian Academy of Science, Chernogolovka, Russia

2 Institute of Radio Engineering and Electronics Russian Academy of Science, Fryazino, Russia

3 Financial University under the Government of Russian Federation, Moscow, Russia

*Address all correspondence to: egorov@iptm.ru

References

[1] Hirsch P, Kellar J. An X-ray micro-beam technique: I-collimation. Proceedings of the Physical Society of London Series B. 1951;**64**:369-374

[2] Spiller E, Segmuller A. Propagation of X-rays in waveguide. Applied Physics Letters. 1974;**24**(2):60-61

[3] Feng Y, Sinha S, Fullerton E, Grubel G, Abernathy D, Siddons D, et al. X-ray Fraunhofer diffraction patterns from a thin film waveguides. Applied Physics Letters. 1995;**67**(24):3647-3649

[4] Lagomarsino S, Jark W, Di Fonzo S, Cedola A, Mueller B, Engstrom P, et al. Submicrometer X-ray beam production by a thin film waveguide. Applied Physics. 1996;**79**(8):4471-4473

[5] Jark W, Di Fonzo S, Lagomarsino S, Cedola A, Di Fabrizio E, Bram A, et al. Properties of a submicrometer X-ray beam at the exit of a waveguide. Applied Physics. 1996;**80**(9):4831-4836

[6] Marton J. The glass tube as X-ray guide. Applied Physics Letters. 1966;**9** (2):194-197

[7] Kumakhov M, Komarov F. Multiple reflection from surface X-ray optics. Physics Reports. 1990;**191**:289-352

[8] Vincze L, Janssens K, Adams F, Ridby A. Detail ray-tracing code for capillary optics. X-ray Spectrometry. 1995;**24**(1):27-37

[9] Arkadiev V, Beloglazov V, Bjeoumikhov A, Gorny H, Langhoff N, Wedell R. Application of capillary optics in modern scientific instrumentation. Poverkhnost. (X-ray, Synchrotron and Neutron Investigations). 2000;**1**:48-54 (in Russian)

[10] Haschke M, Haller M. Examination of poly-capillary lenses for their use in micro-XRF spectrometers. X-ray Spectrometry. 2003;**32**(3):239-247

[11] Rath B, Wang L, Homann B, Gibson W, MacDonald C. Measurements and analysis of radiation effects in polycapillary X-ray optics. Applied Physics. 1998;**83**(12):7424-7425

[12] Mingazin T, Zelenov V, Lejkin V. Slitless collimator for X-ray beams. Instruments and Experimental Techniques. 1981;**24**(1 part 2):244-247

[13] Leykin V, Mingazin T, Zelenov V. Collimating device for X-ray radiation. Pribori i Tekhnika Experimenta. 1981; **24**(3):208-211 (in Russian)

[14] Lejkin V, Mingazin T, Zelenov V. X-ray beam forming by using of a slitless collimator. Instruments and Experimental Techniques. 1984;**27**(6, part 1):1333-1336

[15] Egorov V, Zuev A, Maljukov B. Surface contamination diagnostics of silicon wafers by total reflection X-ray fluorescence spectrometry. Tsvetnaja metallurgija. Izvestija VUZoV. 1997;**5**: 54-69 (in Russian)

[16] Egorov V, Kondratiev O, Zuev A, Egorov E. The modification of TXRF method by use of X-ray slitless collimator. Advances in X-ray Analysis. 2000;**43**:406-417

[17] Zwanenburg M, Peters J, Bongaerts J, de Vries A, Abernathy D, van de Veen J. Propagation of X-ray in a planar waveguide with a turnable air gap. Physical Review Letters. 1999;**82**(8): 1696-1699

[18] Zwanenburg M, van de Veen J, Ficke H, Neerings H. A planar X-ray waveguide with a turnable air gap for the structural investigation of confined fluids. Review of Scientific Instruments. 2000;**71**(4):1723-1732

[19] Kawai J, Harada S, Karimov P. X-ray wave guide and its possible application

to surface analysis. Surface Analysis. 2002;**9**(3):356-358

[20] Pfeiffer T, Salditt P, Hoghoj F, Anderson I, Schell N. X-ray waveguides with multiple guiding layers. Physics Review. 2000;**B62**:16939-16943

[21] Ebel H, Svagera R, Ebel M. Multiple ionization in quantitative XRF. X-ray Spectrometry. 2001;**30**:180-185

[22] Dabagov S. Wave theory of X-ray scattering in capillary structures. X-ray Spectrometry. 2003;**32**:179-185

[23] Fuhse C, Salditt T. Finite-difference field calculations for one-dimensionally confined X-ray waveguides. Physica. 2005;**B357**:57-60

[24] Bukreeva J, Popov A, Pelliceia D, Cedola A, Dabagov S, Logomarsito S. Wave-field formation in a hollow X-ray waveguide. Physical Review Letters. 2006;**97**:184801-1(4)

[25] Pankin S, Hartman A, Salditt T. X-ray propagation in tapered waveguides: Simulation and optimization. Optic Communication. 2008;**281**:2779-2783

[26] Salditt T, Kruger S, Fuhse C, Bahtz C. High transmission planar X-ray waveguide. Physical Review Letters. 2008;**100**:184801-1(4)

[27] Blochin M, Sheitser I. X-ray Handbook. Moscow: Nauka; 1982. 375 p (in Russian)

[28] Zschornack G. Handbook of X-Ray Data. Berlin: Springer; 2007. 969 p

[29] Egorov V, Egorov E. Experimental study of X-ray the energy spectrum formed by a planar waveguide-resonator with specific element reflectors. Advances in X-Ray Analysis. 2006;**v49**:315

[30] Gasnier M, Nevot L. Analysis of crystallographic structures of chromium thin films. Physica Status Solidi. 1981; **A66**:525

[31] Harrick N. Internal Reflection Spectroscopy. New York: InterScience; 1967. 327 p

[32] Egorov V, Egorov E. Ion beam for materials analysis: Conventional and advanced approaches. In: Ahmad I, Maaza M, editors. Ion Beam Application. London: IntechOpen; 2018. 38 p

[33] Doolittle L. Algorithm for the rapid simulation of Rutherford backscattering spectra. Nuclear Instruments and Methods in Physics Research B. 1985;**9**: 344

[34] Turner AJ. Modern state of multilayer optical films field. Physique de Radium. 1950;**11**:444 (in French)

[35] Egorov V, Egorov E. Waveguide-resonance mechanism for X-ray beam propagation: physics and experimental background. Advances in X-ray Analysis. 2003;**46**:307

[36] Egorov V, Egorov E. Background of X-ray nanophotonics based on the planar air waveguide-resonator. X-ray Spectrometry. 2007;**36**:381

[37] Bohm M. Quantum Theory. New York: Prentice-Hall; 1952. 755 p

[38] Blochin M. Physik der Rontgenstrahlung. Berlin: Verlag; 1957. 535 p (in German)

[39] Egorov V, Egorov E. Planar waveguide-resonator: New device for X-ray optics. X-ray Spectrometry. 2004; **33**:360

[40] Landau L, Lifshitz E. Electrodynamics of Continues Medium. Oxford: Pergamon Press; 1984. 586 p

[41] Bedzyk M, Bommarito G, Schildkraud J. X-ray standing waves at a

reflecting mirror surface. Physical Review Letters. 1989;**69**:1376

[42] Goos F, Hanchen H. Novel and fundamental investigation of total internal reflection. Annalen der Physik. 1947;**6**(7–8, part 1):333 (in German)

[43] Snyder A, Love J. Goos-Hanchen shift. Applied Optics. 1976;**15**(1):236

[44] Brekhovskikh L. Waves in Lamellar Medium. New York: Academic Press; 1980. 345 p

[45] Tsuji L, Delalieus F. Characterization of X-ray emerging from between reflector and sample carrier in reflector-assisted TXRF analysis. X-ray Spectrometry. 2004;**33**: 281

[46] Compton A, Allison S. X-Ray in Theory and Experiment. New York: Princeton; 1935. 828 pp

[47] Klug H, Alexander L. X-Ray Diffraction Procedures. New York: Wiley; 1974. 976 pp.

[48] Egorov V, Egorov E. Peculiarities in the formation of X-ray fluxes by waveguide-resonators of different construction. Optics and Spectroscopy. 2018;**124**(6):838

[49] Mandel L, Wolf E. Optical Coherence and Quantum Optics. Cambridge: Cambridge University Press; 1995. 837 p

[50] Egorov V, Egorov E, Loukianchenko E. High effective TXRF spectrometry with waveguide-resonance devices application. Aspects in Mining and Mineral Science. 2018;**2**(4):1

[51] Egorov V, Egorov E, Afanas'ev M. High effective TXRF spectrometry with waveguide-resonance devices application. IOP Series: Journal of Physics: Conference Series. 2018;**1121**: 012011.

[52] Egorov V, Egorov E. Elaboration of pulsed X-ray laser on base of radiation fluxes waveguide-resonance propagation phenomenon. IOP Series: Journal of Physics: Conference Series. 2019;**1396**:012013

[53] Egorov V, Egorov E. About cold fusion possibilities in frame of the waveguide-resonance propagation of radiation fluxes. IOP Series: Journal of Physics: Conference Series. 2019;**1370**: 012021

[54] Kapany N. Fiber Optics: Principles and Application. New York: Academy Press; 1967. 429 p

[55] Shevchenko V. Continues Transition in Optics Waveguides. Boulder, Colorado: Golen Press; 1971. 176 p

[56] Kapany N, Burke J. Optical Waveguides. New York: Academic Press; 1972. 328 p

[57] Markuse D. Theory of Dielectric Optical Waveguides. New York: Academic Press; 1974. 256 p

[58] Unger H. Planar Optical Waveguides and Fibers. Oxford: Clarinton Press; 1977. 771 p

[59] Snyder A, Love J. Optical Waveguide Theory. London: Chapman and Hall Press; 1983. 734 p

[60] Buck J. Fundaments of Optical Fibers. 2nd ed. New York: Wiley; 2004. 352 p

[61] Okamoto K. Fundaments of Optical Waveguides. 2nd ed. New York: Academic Press; 2005. 584 p

[62] Calvo M, Lakshminarayanan V. Optical Waveguides, from Theory to Applied Technologies. New York: CRC Press; 2007. 401 p

[63] Kumar S, Deen M. Fiber Optic Communication. Chichester: Wiley; 2014. 573 p